[4] a) G. Decher, *Science* **1997**, *277*, 1232. b) Y. Lvov, K. Ariga, I. Ichinose, T. Kunitake, *J. Am. Chem. Soc.* **1995**, *117*, 6117. c) P. Hammond, *Curr. Opin. Colloid Interface Sci.* **1999**, *4*, 430. d) H. Mohwald, H. Lichtenfeld, S. Moya, A. Voigt, G.B. Sukhorukov, S. Leporatti, L. Dahne, I. Radtchenko, A. Antipov, C. Gao, *Surfactant Sci. Ser.* **2003**, *109*, 91.

[5] a) M. Antonietti, K. Landfester, *Prog. Polym. Sci., Jpn.* **2002**, *27*, 689. b) M. Antonietti, *Nat. Mater.* **2003**, *2*, 9.

[6] a) Z. Wu, L. Guan, G. Shen, R. Yu, *Analyst (Cambridge, U.K.)* **2002**, *127*, 391. b) S. Park, J. Park, C. Lee, M. Gong, *Sens. Actuators, B* **2002**, *86*, 68. c) A. Diaspro, D. Silvano, S. Krol, O. Cavalleri, A. Gliozzi, *Langmuir* **2002**, *18*, 5047.

[7] a) M. Unger, H.-P. Chou, T. Thorsen, A. Scherer, S. Quake, *Science* **2000**, *288*, 113. b) A. Fu, C. Spence, A. Scherer, F. Arnold, S. Quake, *Nat. Biotechnol.* **1999**, *17*, 1109. c) H. Zheng, I. Lee, M. Rubner, P. Hammond, *Adv. Mater.* **2002**, *14*, 569. d) S. Quake, A. Scherer, *Science* **2000**, *290*, 1536.

[8] a) P. Kenis, R. Ismagilov, G. Whitesides, *Science* **1999**, *285*, 83. b) P. Kenis, R. Ismagilov, S. Takayama, G. Whitesides, S. Li, H. White, *Acc. Chem. Res.* **2000**, *33*, 841. c) S. Takayama, J. McDonald, E. Ostuni, M. N. Liang, P. Kenis, R. Ismagilov, G. Whitesides, *Proc. Natl. Acad. Sci. USA* **1999**, *96*, 5545. d) R. Ferrigno, A. Stroock, T. Clark, M. Mayer, G. Whitesides, *J. Am. Chem. Soc.* **2002**, *124*, 12 930.

[9] L. Kam, S. Boxer, *Langmuir* **2003**, *19*, 1624.

[10] J. Oakey, J. Allely, D. Marr, *Biotechnol. Prog.* **2002**, *18*, 1439.

[11] A. Hatch, A. Kamholz, K. Hawkins, M. Munson, E. Shilling, B. Weigl, P. Yager, *Nat. Biotechnol.* **2001**, *19*, 461.

[12] E. Delamarche, A. Bernard, H. Schmid, A. Bietsch, B. Michel, H. Biebuyck, *J. Am. Chem. Soc.* **1998**, *120*, 500.

[13] S. Takayama, E. Ostuni, P. LeDuc, K. Naruse, D. Ingber, G. Whitesides, *Nature* **2001**, *411*, 1016.

[14] G. Sukhorukov, in *Novel Methods to Study Interfacial Layers* (Eds: D. Möbius, R. Miller), Elsevier, Amsterdam **2001**, pp. 384–415.

[15] G. Ibarz, L. Dahne, E. Donath, H. Möhwald, *Adv. Mater.* **2001**, *14*, 1324.

[16] a) J. Georges, *Spectrochim. Acta, Part A* **2003**, *59*, 519. b) J. Brody, T. Osborn, F. Forster, P. Yager, *Sens. Actuators, A* **1996**, *54*, 704.

High-Conductivity Elastomeric Electronics**

By *Darren S. Gray*, *Joe Tien*, and *Christopher S. Chen**

Flexible electronic circuits have recently gained widespread interest for numerous applications including flexible displays (electronic paper)[1,2] and wearable electronics.[3,4] Despite substantial improvements over rigid devices, current flexible electronics cannot fully conform to their surroundings, due to the inability of metals and conductive polymers to stretch significantly.[5,6] Electronics that could undergo stretching as well as bending would provide additional degrees of freedom in range of motion and prevent damage to both devices and surroundings by matching their mechanical impedances. Currently, to produce a material that is both elastomeric and conductive, metal particles are embedded in an elastomer, such as silicone.[7] This approach is widely used to form interconnections between rigid materials, but the conductivity of such connectors is lower than that of metals and tends to change significantly with strain.[8] Additionally, miniaturization is limited because microfabricated features must be larger than the particle size to ensure conductivity. Here we demonstrate a general strategy to construct elastomeric electronics using microfabricated tortuous wires encased in a silicone elastomer. After a single iteration of geometric optimization, these wires were able to accommodate linear strains of up to 54 % while maintaining stable conductivity. This approach to elastomeric electronics dramatically improves current performance, enabling a range of applications such as forming a direct interface with delicate living tissues or withstanding extreme stress and vibration.

Our strategy for constructing elastomeric electronics is based on the fact that many metals, despite being unable to stretch significantly, are able to bend if their cross sections are sufficiently small. While the common helical spring has been used for centuries to produce a net elongation based on bending, the potential of this simple device to produce stretchable integrated circuits has been largely unexplored. To directly test the hypothesis that integrated circuits made of springs could form the basis of stretchable elastomeric electronics, we used standard lithography techniques[9–11] to embed straight or spring-shaped metal wires in an elastomer (Fig. 1). Circuits, formed by connecting a conductivity meter to exposed contact pads at the ends of the wires, were subjected to linear strain until the point of electrical failure (strain at failure). For ease of microscale manufacture, springs were fabricated in the form of 2D oscillations instead of 3D coils. Gold was the chosen metal, based on its high conductivity, malleability, and chemical inertness.[12] Poly(dimethylsiloxane) (PDMS) was chosen to form the elastomeric "circuit board," mechanically protecting and electrically insulating the wires, based on its durability, adjustable stiffness, biocompatibility, and commercial availability as an insulating compound.[11,13]

When straight wires were strained even minimally (2.4 ± 0.5 %), macroscopic fractures interrupted the flow of current (Fig. 2a, left). Upon allowing the gold wires and their encasing PDMS to return to a strain-free state, the wires regained conductivity, in accordance with the observed return of metal–metal contact at the fracture site. Tortuous wires, containing a wave formed of linked half-ellipses with an amplitude of half the magnitude of the period, remained conductive at a much greater strain of 14.2 ± 0.5 % (Fig. 2a, center). The strain at electronic failure was further improved to

[*] Prof. C. S. Chen, D. S. Gray
Departments of Biomedical Engineering and Oncology
Johns Hopkins University
720 Rutland Avenue, Baltimore, MD 21205 (USA)
E-mail: cchen@bme.jhu.edu
Prof. J. Tien
Department of Biomedical Engineering, Boston University
44 Cummington Street, Boston, MA 02215 (USA)

[**] We gratefully acknowledge funding from the Whitaker Foundation, NIBIB (EB 00262), The Office of Naval Research, and DARPA. We thank Celeste M. Nelson, Srivatsan Raghavan, and John L. Tan for discussions.

DOI: 10.1002/adma.200306107

ADVANCED MATERIALS

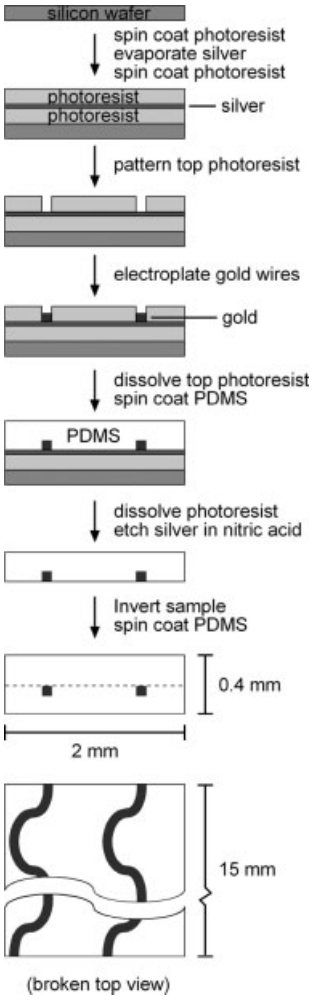

Figure 1. Construction of elastomeric wires. Schematic of the micro-fabrication process used to generate tortuous gold wires encased in a thin PDMS backing. All illustrations are side views, except the final product, which is also shown as a broken top view. Drawings are not to scale.

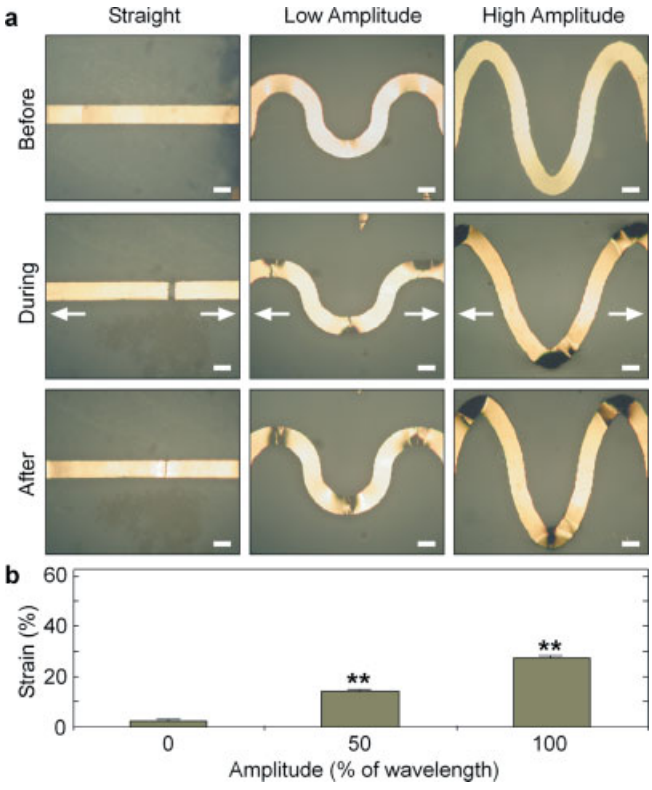

Figure 2. Tensile strain testing of metal wires embedded in elastomer. a) Bright-field reflected light micrographs of elastomer-embedded gold wires with tortuosities of different amplitudes before, during, and after the strain at electrical failure. Wires appear dark in regions of out-of-plane buckling. Arrows indicate the direction of applied strain. Scale bars are 100 μm. b) Graph of the strain at electrical failure for different amplitudes of tortuosity. Elastomer-embedded metal wires with higher amplitudes endured higher strains than less tortuous wires. Error bars indicate standard error of the mean. ** Indicates $p < 0.0001$ versus neighboring bar(s).

27.2 ± 0.9 % simply by doubling the amplitude–wavelength ratio (Fig. 2a, right). Again, conductivity recovered upon removal of the strain. For the tortuous wires, fractures typically formed at the peak and trough of each wave, indicating that stresses were concentrated at these regions. Out-of-plane buckling, seen as dark regions on the wires, is also indicative of stress.[14] The buckling probably resulted from the greater ability of the wires to bend in their thinnest dimension, perpendicular to the plane of the wire. Together, these findings confirm that tortuosity increases the ability of wires to elongate, because metal bends more readily than it stretches.

Since our early experiments demonstrated that the strain at failure was influenced by the geometry of wire tortuosity, we explored how several other geometric parameters might affect the strain that the wires could withstand. Firstly, wire width was reduced from 100 μm to 10 μm. Narrow wires stretched more than wide wires (Fig. 3a), presumably because of reduced stress concentration at the peaks and troughs of the waves. Adding multiple adjacent wires, despite their redundant current paths, did not change the strain at failure relative to single wires, suggesting that all the wires generally fail within a narrow range of strain (Fig. 3b). Nonetheless, multiple wires were used for subsequent testing due to the desirability of their increased current capacity. To vary the absolute magnitude of the tortuosities, we reduced the wavelength and amplitude in tandem, maintaining a fixed amplitude–wavelength ratio. Strain at failure increased dramatically in small versus large tortuosities (Fig. 3c), despite their identical amplitude–wavelength ratio. This effect appears to occur because the peak and trough regions of the larger tortuosities have a longer arc length, and thus locally approximate straight wires, already shown to be susceptible to failure under tension. Interestingly, the addition of redundant current paths by overlapping the wires decreased rather than increased the strain at failure (Fig. 3d). Wires that overlapped each other or actually crossed were found to fracture at the junctions, suggesting that such junctions constrained the unbending of the wires and introduced regions of stress concentration. When the depth of the wires was reduced to facilitate bending perpendicular to the plane of the elastomer, a small but significant

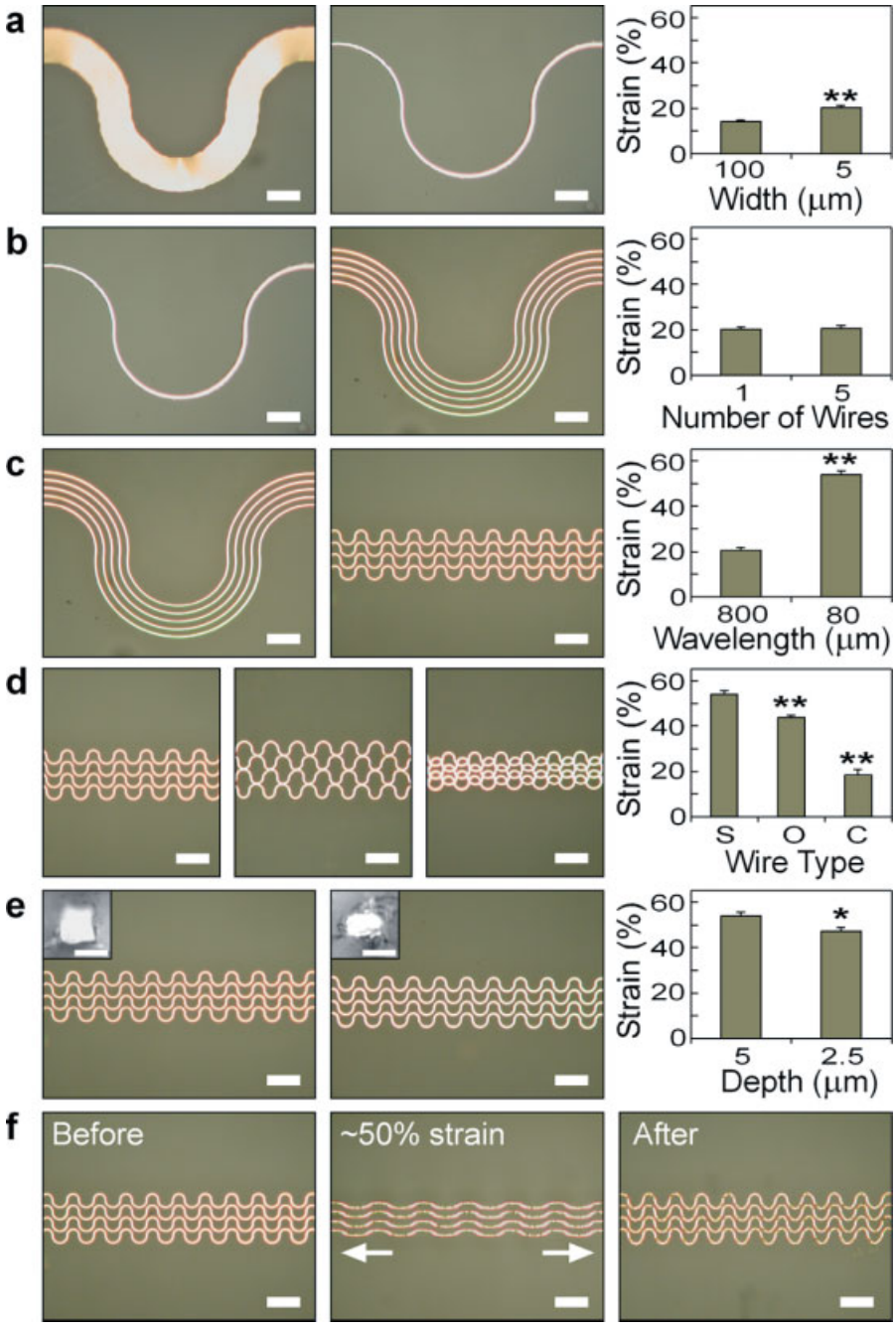

Figure 3. Role of wire geometry in strain at electrical failure. a) Wide wires, shown unstrained in the left panel, are compared to narrow wires, shown unstrained in the center panel. The graph in the right panel shows that narrow wires elongate more than wide wires before electrical failure. b) Single wires (left panel) elongate as much as multiple wires (center panel). c) Wires with tortuosities of larger wavelength (left panel) elongate less than wires of smaller wavelength with the same wavelength–amplitude ratio (center panel). d) Separate wires (S, left panel) elongate more than overlapping wires (O, left center panel), which elongate more than crossed wires (C, right center panel). e) Deeper wires (left panel) elongate more than shallower wires (center panel). Insets show further magnified views of wire cross-sections. f) The wires with the highest strain at electrical failure (left panel) were examined near this level of strain (center panel), and after the strain was released (right panel). Arrows indicate direction of applied strain. All photos were acquired using bright-field reflected light microscopy. Error bars indicate standard error of the mean. * Indicates $p < 0.02$ versus neighboring bar(s). ** Indicates $p < 0.0001$ versus neighboring bar(s). Main panel scale bars indicate 100 μm. Inset scale bars indicate 5 μm.

decrease in maximum linear strain occurred in shallow versus deep wires (Fig. 3e). Presumably, the shallow wires were made more fragile without increasing their ability to elongate in the direction of applied strain.

For the best geometry tested—narrow wires with many tortuosities—we examined the wires near the strain at failure (Fig. 3f). Typically, failure occurred when a single crack formed at a random location along each wire. Remarkably, the 54 ± 2 % strain achieved with these wires approaches the 57 % strain theoretically calculated as occurring if the wires were fully straightened without actual elongation. By selecting an appropriate geometry, we have achieved nearly total unbending of tortuous metal wires encased in elastomer. Upon release of the applied strain, these wires returned nearly to their initial shape. Importantly, wire conductivity was not dramatically altered by sub-failure strain.

Although the strain at failure provided a convenient method of optimizing wire geometry, many applications would require wires to stretch repeatedly. To further analyze the best wires, we subjected them to 25 % cyclic strain, approximately half their experimental strain at failure. Samples, each having four wires with cross sections of 5 μm × 5 μm, and tortuosities with amplitudes of 40 μm and wavelengths of 80 μm, withstood 200 ± 30 cycles of strain. Assuming the standard exponential relationship between strain and fatigue life, one predicts that these wires should withstand approximately 5000 cycles at 10 % strain, 70 000 cycles at 5 % strain, and 2 000 000 cycles at 2 % strain.[15]

As a demonstration of the mechanical stability of our wires, we constructed a simple circuit made of tortuous wires, a light-emitting diode (LED), and a battery on a PDMS backing (Fig. 4a). When the circuit was manually stretched to ~25 % strain several times, the LED remained lit, indicating that the wires

ADVANCED MATERIALS

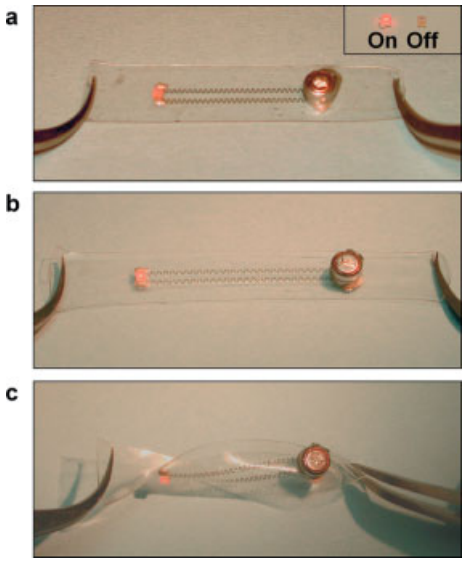

Figure 4. Deformation of a working elastomeric circuit. a) Photograph of elastomeric circuit composed of a power source connected to an LED via elastomeric wires. The circuit was held manually by forceps later used to apply strains. b) Photograph of the elastomeric circuit undergoing tensile strain. c) Photograph of the elastomeric circuit undergoing torsional strain.

were still conductive (Fig. 4b). The LED also remained lit as the circuit was twisted through more than 180° (Fig. 4c). In this demonstration, wide, high-amplitude wires (Fig. 2a, right) were used for visualization. One would expect even better flexibility of the system using the most flexible wires (Fig. 3f), which exhibited nearly two-fold better mechanical performance.

Despite the dramatic strains achieved in this work, the tortuous wire strategy could be further optimized. The finding that smaller tortuosities outperformed larger tortuosities implies that further miniaturization could improve the elastomeric wires. Tortuosities of smaller wavelength could be superimposed on the bends currently present in order to promote stretch in multiple dimensions and improve the strain at failure by increasing arc length. To further increase arc length, undulations also could be added in the *z*-direction, parallel to the plane of the circuit,[16] or wires could be made in the form of 3D coil springs, by adapting advanced fabrication methods.[17–19] In order to achieve more cycles before failure, a more fatigue-resistant metal[20] or a flexible polymeric conductor[21–23] could be used, and the stiffness of the elastomer encasing the wires could be varied to control circuit stiffness. These approaches might even be extended to produce components that stretched in addition to their connecting wires.

Ultimately, the strategy of constructing stretchable electronics using elastomer-encased tortuous wires could enable working circuits to withstand unprecedented degrees of bending, stretching, shock, and vibration. For example, electronics within elastic clothing could monitor athletic or combat performance while allowing the wearer great freedom of movement. In addition to operating in environments that would damage more rigid circuits, elastomeric electronics could interface safely and directly with delicate biological tissues. For example, pliable artificial nerves could stretch along with muscles, elastomeric sensors in direct contact with large regions of the surface of the heart could accurately monitor cardiac performance, and highly pliant electrodes could safely conform to the surface of the brain during cranial pulsations. We believe that the basic understanding of stretchable wires developed in this work constitutes a significant development towards facilitating these and other applications through fully functional elastomeric electronics.

Experimental

To construct elastomeric circuits, silicon wafers were spin-coated with photoresist (Microposit S1813, Shipley) followed by e-beam evaporation of 50 Å of Ti and 1000 Å of Ag (Fig. 1). To form wires, Au was electroplated onto the Ag through a patterned layer of photoresist (Microposit SJR5440, Shipley); the photoresist was removed subsequently with rinses of toluene, acetone, and ethanol. After brushing with an adhesion primer (92-023, Dow Corning), the circuits were spin-coated with PDMS (Sylgard 184, Dow Corning). Circuits were lifted off the wafers by sonication in ethanol, followed by removal of the silver with 8 M nitric acid. To encase the wires, circuits were inverted, placed on new wafers for mechanical support, and spin-coated with a second layer of PDMS, with non-encased regions to be used for contacts temporarily covered by glass cover slips.

To determine the linear tensile strain at which wires became non-conductive (strain at failure), a uniaxial strain testing device was outfitted with an electrical continuity tester, which made electrical contact with both wire ends. At least 11 samples of each type were stretched uniaxially at a strain rate of 0.01 s^{-1} until they became non-conductive. For cyclical testing, four samples were subjected to cyclic strain at 1 Hz until they became non-conductive as defined by a resistance measurement > 100 Ω. Statistics comparing different wire types were computed using Student's t-Test.

Received: September 2, 2003
Published online: February 18, 2004

[1] J. A. Rogers, Z. Bao, K. Baldwin, A. Dodabalapur, B. Crone, V. R. Raju, V. Kuck, H. Katz, K. Amundson, J. Ewing, P. Drzaic, *Proc. Natl. Acad. Sci. USA* **2001**, *98*, 4835.
[2] Y. Chen, J. Au, P. Kazlas, A. Ritenour, H. Gates, M. McCreary, *Nature* **2003**, *423*, 136.
[3] R. Gregory, W. Kimbrell, H. Kuhn, *Synth. Met.* **1989**, *28*, 823.
[4] E. R. Post, M. Orth, P. R. Russo, N. Gershenfeld, *IBM Syst. J.* **2000**, *39*, 840.
[5] S. Yang, E. Ruckenstein, *Synth. Met.* **1993**, *60*, 249.
[6] T. Saito, T. Furuta, J.-H. Hwang, S. Kuramoto, K. Nishino, N. Suzuki, R. Chen, A. Yamada, K. Ito, Y. Seno, T. Nonaka, H. Ikehata, N. Nagasako, C. Iwamoto, Y. Ikuhara, T. Sakuma, *Science* **2003**, *300*, 464.
[7] J. Xie, M. Pecht, D. DeDonato, A. Hassanzadeh, *Microelectron. Reliab.* **2001**, *21*, 281.
[8] T. Tamai, *IEEE Trans. Compon., Hybrids, Manuf. Technol.* **1982**, *5*, 56.
[9] G. Chiu, J. Shaw, *IBM J. Res. Dev.* **1997**, *41*, 3.
[10] M. Madou, *Lithography*, CRC Press, Boca Raton, FL **1997**.
[11] G. M. Whitesides, E. Ostuni, S. Takayama, X. Jiang, D. E. Ingber, *Annu. Rev. Biomed. Eng.* **2001**, *3*, 335.
[12] M. Hunt, *Mater. Eng.* **1990**, *107*, 17.

[13] N. Q. Balaban, U. S. Schwarz, D. Riveline, P. Goichberg, G. Tzur, I. Sabanay, D. Mahalu, S. Safran, A. Bershadsky, L. Addadi, B. Geiger, *Nat. Cell Biol.* **2001**, *3*, 466.
[14] W. Huck, N. Bowden, P. Onck, T. Pardoen, J. Hutchinson, G. M. Whitesides, *Langmuir* **2000**, *16*, 3497.
[15] F. Ellyin, *Fatigue Damage, Crack Growth and Life Prediction*, Chapman & Hall, New York **1997**.
[16] S. Lacour, S. Wagner, Z. Huang, Z. Sou, *Appl. Phys. Lett.* **2003**, *82*, 2404.
[17] K. Ikuta, K. Hirowatatari, in *Proc. IEEE Micro Electro Mechanical Systems (MEMS '93)*, IEEE, Piscatawney, NJ **1993**, p. 42.
[18] J. R. Anderson, D. T. Chiu, R. J. Jackman, O. Cherniavskaya, J. C. McDonald, H. Wu, S. H. Whitesides, G. M. Whitesides, *Anal. Chem.* **2000**, *72*, 3158.
[19] R. J. Jackman, S. T. Brittain, A. Adams, M. G. Prentiss, G. M. Whitesides, *Science* **1998**, *280*, 2089.
[20] V. Birman, *Appl. Mech. Rev.* **1997**, *50*, 629.
[21] H. Shirakawa, E. Louis, A. MacDiarmid, C. Chiang, A. Heeger, *J. Chem. Soc., Chem. Commun.* **1977**, *579*, 578.
[22] C. Drury, C. Mutsaers, C. Hart, M. Matters, D. D. M. de Leeuw, *Appl. Phys. Lett.* **1998**, *73*, 108.
[23] S. Holdcroft, *Adv. Mater.* **2001**, *13*, 1753.

Material Storage Mechanism in Porous Nanocarbon**

By *Kumiko Ajima*, *Masako Yudasaka*, *Kazu Suenaga*,* *Daisuke Kasuya*, *Takeshi Azami*, and *Sumio Iijima*

Carbonaceous materials, such as activated carbon and charcoal, have long been known to possess "nanospaces," where a variety of materials can be accommodated. Their structures and chemical properties, however, have never been optimized for any specific purpose, because their mechanism of storing objects is not yet fully understood. We have therefore attempted to visualize how material is stored in the inner spaces of nanocarbon materials in order to verify the storage mechanism. We used "single-walled carbon nanohorns" (SWNHs)[1] for this purpose. This porous nanocarbon material, composed of single-layer graphite walls, is known to possess completely enclosed nanoscale spaces, and is therefore quite suitable for these experiments. Figure 1a shows intact SWNHs with the nanospaces inside. Each nanohorn's diameter varies from 1 nm at the tip to 5 nm at the wide end, and they have a longitudinal axis of the order of tens of nanometers. Hundreds of nanohorns combine to make an aggregate which resembles a dahlia flower (Fig. 1a left). This dahlia-like aggregate of SWNHs is an ideal test object to elucidate the storage mechanism, since it is full of closed spaces and includes structural variations.

We attempted to introduce a path from the outside into the nanospace by means of strictly controlled heat treatments in oxygen gas. As can be seen in Figure 1a, bumps and dips (as indicated by arrows) are often found on the graphite walls of carbon nanohorns before heat treatment. They are believed to incorporate the disclination defects of graphite walls, such as pentagon and heptagon rings, to achieve a complete closure of the graphitic network. Similar bumps and dips have been reported in carbon nanotubes[2] and the oxidation of nanotubes is known to start with such topological defects in the graphite networks due to the strain field they introduce.[3–5] Therefore, it is reasonable to assume that the paths into the nanospaces within the nanohorns are first introduced at the disclination defects seen in the intact nanohorns (Fig. 1a).

Figure 1b shows high-resolution transmission electron microscopic (HRTEM) images featuring heat-treated SWNHs with paths opened to the inside space. Two types of path can be found: a path at the tip, and a path on the side-wall of the nanohorn (Fig. 1b, left and right, respectively). The HRTEM image simulation (Fig. 1c) was carried out in order to corroborate the size and structure of the paths, and was exactly matched to the observation conditions. The simulated images agree quite well with the observed HRTEM images of the nanohorn, with holes (paths) present at the tip or on the side-wall. The size distributions of the observed paths at the tip and on the side-wall were obtained from hundreds of HRTEM images (Fig. 2). The dominant path size is 0.5 to 1.0 nm in both cases. The path at the tip has a narrow size distribution of around 0.5–1.5 nm, while the path size for the side wall has a much wider range of up to several nanometers. Therefore it is assumed that, generally speaking, only materials of a size smaller than 1.5 nm could travel through these paths and be accommodated inside the nanospaces.

Various molecules could enter porous nanocarbon material made of graphite layers containing open paths. We will present results for the entrance of fullerene (C_{60}) molecules (which are approximately 0.7 nm in diameter), since they are easily distinguishable by electron microscopy.[6] It was very important to choose such a distinctive molecule for the HRTEM observation in order to make a quantitative analysis of the number of adsorbed molecules. It has been repeatedly reported that fullerene molecules will percolate into many kinds of porous nanocarbon materials. Because the molecules are easy to sublimate, and also soluble in many solvents, we were able to introduce them into carbonaceous materials both in gas phase and liquid phase.[7–9]

Figure 3 shows HRTEM images of the open-path carbon nanohorns after insertion of the fullerene molecules by a liq-

[*] Dr. K. Suenaga, Prof. S. Iijima
National Institute of Advanced Industrial Science and Technology (AIST)
Tukuba, 305–8565 (Japan)
E-mail: suenaga-kazu@aist.go.jp
K. Ajima, Dr. M. Yudasaka
Japan Science and Technology Corporation, NEC Corporation
Tsukuba 305–8501 (Japan)
Dr. D. Kasuya, Dr. T. Azami
NEC Corporation
Tsukuba 305–8501 (Japan)
[**] This work is partially supported by the NEDO Nanocarbon Technology project.

DOI: 10.1002/adma.200306142